Thermal Gradients and Thermal Conductivity in PEM Fuel Cells, Compared to Li-ion Batteries and Super Capacitors

Odne S. Burheim[a] and Bruno G. Pollet[a]

[a]Department of Energy and Process Engineering, Norwegian University of Science and Technology (NTNU), Trondheim 7491, Norway

The PEMFC has been developed into a very effective energy converter. That is, the PEMFC offers high power at the same energy efficiency range. This is because the cell potential remains constant while current density increases. With increased current density at constant energy efficiency, the heat flux increases along with internal temperature gradients. During the last 15 years, several studies of the thermal conductivity of PEMFC components have been undertaken. The knowledge now covers PTFE loading, ageing, water content, direction (in- vs. through-plane), material types, and material integration. With a modern fuel cell operation at a cell voltage of +0.7 V, one can easily observe temperature differences between the polarisation plates and the membrane of more than 10^{o}C, depending upon the state of the water and material selection.
In other electrochemical energy storage devices such as supercapacitors (SC) and lithium ion batteries (LiB), thermal conductivity values are similar to those of the PEMFC. From an engineering point of view, it is interesting to compare thermal gradients and internal temperature differences of a PEMFC to LiB and SC. The thermal conductivity of the materials are similar, the operation voltage is higher in a LiB and SC than in a PEMFC, the electrode thicknesses are larger in a LiB and SC than in a PEMFC; there are less opportunities for cooling inside a LiB and SC than in a PEMFC, and remarkably, relevant current density of a PEMFC, SC, and LiB are 30 000, 200, and 50 A m^{-2}, respectively.

Introduction

Energy storage is as important to the energy economy as banking is to the monetary one. When transitioning from a fossil fuel based economy to a renewable one, chemical energy supply is replaced by electrical energy supply. Electric energy needs to be stored and changed into a form that can be useful in the transport sector (1). In the transport sector, hydrogen PEMFC, LiB and SC are often pointed at as technologies that can fit into this category, providing power and energy when and where it is needed.

From an engineering point of view, and especially a thermodynamic one, evaluating both heat and power of these devices is of interest. Power is interesting as it is the useful part of the energy, while heat is of interest for designing cooling systems. Controlling the operation temperature and temperature distribution of these technologies is important primarily for performance, but also for long term durability.

There is in particular three denominators that makes comparing thermal gradients in the PEMFC, LiB and SC interesting. One, because of the exponential increase of the electrolyte conductivity with temperature, power density of the electrochemical systems increase with temperature. Two, as most degradation mechanisms are related to classical reaction mechanisms and the reaction rate constants typically also follow an Arrhenius behaviour (exp[aT]); degradation rates also increases with temperature. Three, all the technologies relies upon having large active surface area per electrode volume, which in turn leads to low thermal conductivity. Beyond these three similarities, the the three technologies differ a lot in design. They also differ in conversion rates (current density). The difference in geometry and rates alongside the other similarities therefore constitute a very interesting and meaningful case to study.

PEMFC

The polymer electrolyte membrane fuel cell or proton exchange membrane fuel cell (PEMFC) uses pure hydrogen as a fuel on the anode, and oxygen from the air on the cathode. Hydrogen splits into protons and electrons at the anode. Protons migrate through the membrane (polymer electrolyte) and the electrons pass externally in an electronic circuit. At the cathode the two recombine together with oxygen to form water. In this process, chemical energy is converted into electric power and heat. A PEMFC consists of several components with a total thickness of up to a few millimetres, before stacked with cooling channels in between each cell. A sketch of a PEMFC is provided in Fig. 1.

Because of the high energy density of hydrogen (33 kWh/kg), fast fuelling time (2-3 minutes of a car), and good power density (1 kW/kg), hydrogen PEMFCs are well suited for the transport sector where large distances are to be covered (cars, trucks, trains, passenger speed boats etc) or when continuous operation is required (forklifts). Another market for hydrogen PEMFC is in back up power systems because the system can start up extremely fast, last for as long as there is hydrogen, and have energy stored for a long time in the form of hydrogen.

Heat management and temperature distribution is important in engineering systems around a PEMFC (2). Once a high power fuel cell is designed, the produced water needs to be removed along with the heat (3). A PEMFC operating in the temperature range of 70-90 ^{o}C, experience a great variety of water behaviour, as the water vapour pressure increases from 0.31 to 0.70 bar, meaning that the water is more easily condensed at lower temperatures. Large amounts of water in the PEMFC at low temperature can create flooding and impede oxygen access, and high temperature can create local dry out and possible delamination of the PEMFC sub-components (membrane electrode assemblies - MEAs) (4). Moreover, different thermal mechanisms also increase degradation mechanisms in the catalyst layer (CL) (5).

LiB

The secondary lithium ion battery (LiB) is based upon having a two-electrode rechargeable setup, where the cathode typically consists of a mix of lithium oxides and other transition metal oxides and the anode consists of carbon particles loaded with dissolved lithium metal. At the anode, the lithium is oxidised into lithium ions and electrons, where the lithium ions migrate to the cathode via an organic solvent based electrolyte (in a porous electrode separator) and the electrons move in an external electronic

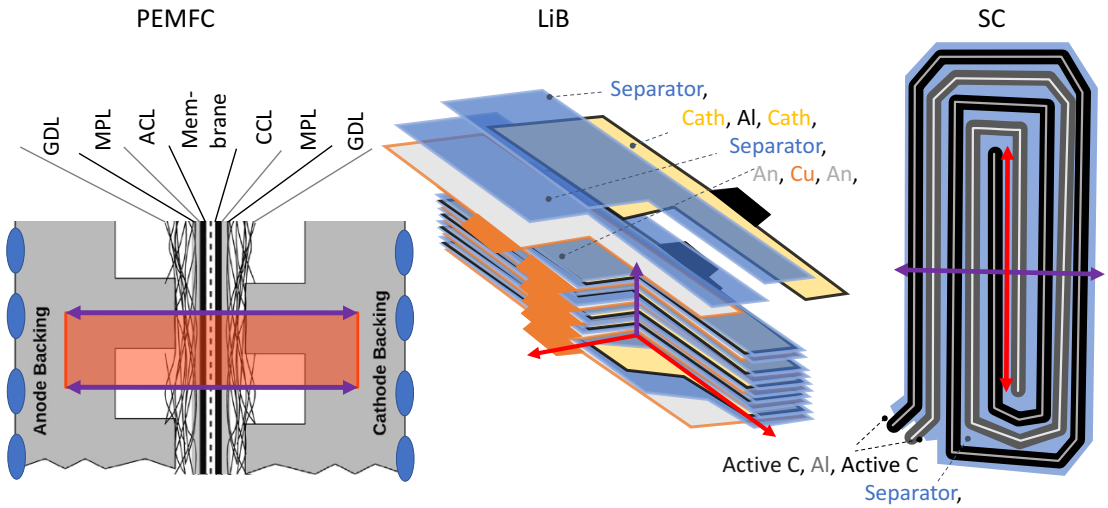

Figure 1. Overview of selected technology geometry for the present study for PEM fuel cell (PEMFC), lithium ion battery (LiB), and supercapacitor (SC).

circuit. At the cathode the transition metal undergoes a reduction in oxidation number and meets the electroneutrality balance by receiving the electron and lithium ion. The cells are assembled by smearing a cathode layer $\geq$ 80 μm on each side of a 25-30 μm aluminium film and the anode likewise on a copper foil, albeit typically $\sim$20% thicker than the cathode one. Because of this, large battery cells are typically 2-5 mm thick with 10-20 cells stacked in a repeating symmetric manner (Cu-An-Separator-Cath-Al-Cath-Sep-An-Cu-An-etc.). A sketch of a LiB poach cell is given in Fig. 1.

LiB is most widely used in consumer electronics where mild charging and discharging cycles takes place. Over the past 5-10 years, they have also become much more used in light vehicles like urban passenger vehicles, where charging in half an hour and discharging in 2 hours has become relevant. In hybrid systems the charging cycles can be even more intense and in large ships, where batteries are accounted for as spinning reserve, discharge rates down to 8 minutes and charging rates down to 20 minutes is needed. In the automotive sector, battery packs have become larger due to the increase in energy demand. Thus thermal gradients have also increased.

The most important factor for ageing or degradation of LiB is the increase in temperature. (6, 7) Secondly, it is the state of charge (SoC). Thirdly, it is the discharge rate, before charging rate. From the perspective of temperature being so important for ageing and degradation, it is clear why thermal gradients is so relevant.

SC

Supercapacitors (SC) do not include red-ox reactions, rather they store energy in the form of local deviation from electroneutrality. When passing charges through a SC, the ionic species near the electrode surface pass charge over to the other electrode. In this way, the electrolyte near the negatively charged electrode has a surplus of positive ions. Similarly, the electrolyte near the positively charged electrode has a surplus of anions. This region of iunbalanced electroneutrality is termed the double layer (DL), and is typically 1-10 nm in thickness. The most common material is a porous carbon, where the pores are as small as a few nano meters. These pores are in turn made of carbon particles that are very similar to a PEMFC catalyst layer and LiB anode material. (8) A

sketch of a SC folded as a poach cell is provided in Fig. 1.

SCs are typically used in systems that need high power for short periods and where they can be quickly charged. Examples can be buses that charge on every bus stop, cranes lifting and lowering freight with a high frequency. Other areas of use is when little energy is required, like for small LED lamps that are charged with simple hand power. Because there is no red-ox reaction, SCs can have very high energy efficiency, as the only energy lost is of "Ohmic nature".

SCs operate at very high rates and for longer times, with full charging cycles taking place in the time frame of minutes. The cell voltage is much beyond the electrochemical splitting of water, so organic electrolytes are used, in principle not very different from those in LiBs. Therefore, and as long as the potential does not exceed the oxidation potential of the electrolyte, the increase in temperature is the most important factor for ageing and degradation.

Systems Thermal Conductivity and Geometry

The three technologies, PEMFC, LiB and SC have some similarities in their geometric design, in that they are prismatic and have rather large aspect ratios. Sketches of the three technologies are given in Fig. 1. These are geometries that are typical for large units and will be explained in greater detail in the following sub-sections.

One thing that all these designs have in common is that when the aspect ratio is large enough, the device becomes isothermal in two of the directions (indicated red) and thus allows for one dimensional modelling (indicated purple), or at least to have planar isothermal boundary conditions. The space component where we, in the end, compare thermal gradients (purple) is termed the *through-plane* direction, whereas the two space components perpendicular to this is termed the *in-plane* components.

PEMFC

The PEMFC is designed as shown in Fig. 1, where the different layers of sub-components are sandwiched between to backings, also known as polarisation or flow field or bipolar plates. The backing plates can consist of double layered materials with cooling in between, as is indicated by the blue ovals in the figure. Some PEMFCs are air cooled, however it is the double plate backing that is considered here, because it is common and because it makes thermal modelling much more trivial (simple representative models is sought here).

Thermal conductivity measurements of PEMFC components have been carefully investigated over the last 10-15 years (9–28) and it is well summarised in (29). Other relevant reviews of thermal modelling and gradients of PEMFC and sub-components are (2, 30, 31). A table of relevant physical thermal properties for the modelling of a PEMFC thermal gradients is given in Table I.

The first value in Table I considers the backing plate of the PEMFC. The backing can change in thickness and is typically carbon or stainless steel. The combination of high thermal conductivity and rather thick layers makes this component closest to isothermal among the PEMFC components. The next layer is the contact between the backing and the GDL, which is typically equivalent to a layer of air with the thickness

TABLE I. PEMFC thermal conductivity values range in the literature and values used in the present thermal model.

Material	$\mathbf{k_{range}}$ **/ W K^{-1}m^{-1}**	δ_i **/** μ**m**	**Refs**	**k,** δ_{used}
Dry:				
Backing	10-300	$\geq$1000	(32)	100, 2000
$GDL_{cont.}$	0.025	5-20	(12)	0.025, 10
$GDL_{in-pl.}$	0.15-0.9	150-350	(9, 10, 12)	0.35, 250
$GDL_{thr.-pl.}$	1-10	"∞"	(14–17)	5, —
MPL	0.07-0.11	20-70	(21)	0.09, 50
CL	0.07-0.22	10-20	(23, 27)	0.15, 10/20*
Membrane	0.17-0.26	25-125	(10, 13)	0.22, 30
Watered	k_{wet}=(2-3)k_{dry}		(12, 13, 21, 23)	k_{wet}=2.5k_{dry}

*Anode CL / Cathode CL. GDL is Gas Diffusion Layer

TABLE II. LiB thermal conductivity values range in the literature and values used in the present thermal modell.

Material	$\mathbf{k_{range}}$ **/ W K^{-1}m^{-1}**	δ_i **/** μ**m**	**Refs**	**k,** δ_{used}
Dry:				
Anode CC, (Cu)	380-400	25-30	(39)	390, 30
Anode AM	0.1-0.7	90-110	(34, 35)	0.35, 95
Cathode CC (Al)	230-250	25-30	(39)	240, 30
Cathode AM	0.2-0.5	75-95	(34, 35)	0.35, 80
Separator	0.1-0.5	20-30	(34, 35)	0.2, 20
Electrolyte	k_{wet}=(2-3)k_{dry}		(12, 13, 21, 23)	k_{wet}=2.5k_{dry}

AM denotes Active Material. CC denotes Current Collector.

of a GDL fibre. When water is present, the thermal resistance is more like that of water, which is 20 times smaller ($k_{water} = 20 \cdot k_{air}$). The GDL thermal conductivity changes a lot between different types of materials, compaction pressure and PTFE content, but the frequently used SigracetXXBA has intermediate values and is chosen for the present model. The MPL and CL thermal conductivity when measured for self standing materials is low ($\approx$0.1 W /Km), however analyses of MPL on top of a GDL suggest 2-3 times larger values, which is due to the interference between the MPL and GDL (20–22). In the present model we use the values obtained for the self standing MPL. For the CL, the thermal conductivity value used is one between the two studies found in the literature (23, 27). The selected thermal conductivity refers to one where the membrane is partly in contact with water. When water is present, the thermal conductivity of the GDL, MPL, and CL increase by a factor between 2 and 3. For simplicity, a factor of 2.5 is used for all layers here.

LiB

Lithium ion batteries (LiB) have received much less attention when it comes to considering thermal conductivity, relatively to the PEMFC area. (33) Some studies report measurements of the single components that constitute a LiB (7, 34–36) and others on the entire poach cell (37), or both (38–42). Also modelling by a lattice Boltzman approach has been reported to be in fair agreement with experimental studies (43). Similarly to PEMFC materials, the porous electrode materials soaked in a liquid appear to have a 2-3 times higher thermal conductivity than the dry ones. The separator on the other hand can change by a factor from 1-6, depending on the separator types and fabrics. For simplicity and since the objective here is to compare the technologies, we also use the factor of 2.5 between thermal conductivity of dry and soaked materials. An overview of selected values in the present model is given in Table II

TABLE III. SC thermal conductivity values range in the literature and values used in the present thermal modell.

Material	$\mathbf{k_{range}}$ **/ W K^{-1}m^{-1}**	δ_i **/** μ**m**	**Refs**	**k,** δ_{used}
Dry:				
Electrode CC, (Al)	200-250	25-30	(32)	200, 30
Electrode AM	0.1-0.15	90-100	(44, 45, 47)	0.15, 95
Separator	0.2-0.25	60-70	(44)	0.2, 25
Electrolyte	k_{wet}=(2-3)k_{dry}		(12, 13, 21, 23)	k_{wet}=2.5k_{dry}

*

SC

Supercapacitor (SC) thermal conductivity values have a lot in common with LiB ones, in that (i) they are scarcely investigated and (ii) they are very similar to LiB anodes and separators (44, 45). Experimental studies of thermal conductivity is scarce, however several studies where thermocouples are attached on the outside of SC devices used to assess some empirical cell thermal diffusivity and conductivty are reported (46).

Model Considerations

In the presented models, Fourier's first law is solved for two dimensions using a continuum model approach where the different domains are given uniform heat sources and thermal conductivity. This is carried out using the commercial software COMSOL Multiphysics 5.2 basic module and a finite element Method (FEM). The domains are made in a rectangular shape with second order meshing, which means that the different domains do not need sub-meshing to obtain a valid solution. Thus the modelling requires extremely little computational resources. The values given to the different domains are given in Tables I, II, III, and IV. In presenting the results, temperature profiles form the purple lines in Fig.1 are extracted from COMSOL Mutliphysics and plotted.

Table IV gives the heat sources of the different systems used in the present models. In a PEMFC, the reversible and entropic heat relate to the entropy change of the reaction and the adsorption of gases (48, 49). When multiplying an entropy value with temperature it becomes an energy term, J. When dividing by the Faraday constant it becomes a voltage term, V. When dividing the half cell entropy term with the Faraday constant, it becomes the Seebeck coefficient, V/K. In the context of this, we give the reversible heats as voltage terms. The resistance of the membrane is taken from (50) and the Tafel kinetics from (51). For the LiB, the reversible heat of the symmetry cell of the two lithium cobalt oxide (LCO) electrodes were recently reported for the first time (52). It is a time dependent value, but when considering a full cycle discharge time of 20 minutes (3C, equivalent to $\approx$60 A m^{-2} (45)), the initial values are the relevant ones. The Ohmic heat in a LiB is based on measuring a commercial poach cell, and attributed only to the separator region. The LiB Tafel heat is attributed to the cathode. The cell considered in the model consists of 24 cells in parallel inside a battery pouch, as sketched in Fig. 1. Because of the symmetry of the mid-plane in the layered stack, only half of the stack is modelled and presented. The entire thickness of the pouch is around 6-7mm thick. The same about the geometry goes for the SC. SC on the other hand have very few irreversible heat terms and are subject to charging and discharging cycles so intense that the reversible heat effects (entropic) can be disregarded in a thermal model. This is as they act as a cooling term when charging and heating terms when

TABLE IV. PEMFC, LiB, and SC heat sources overview.

Nature	**Location**	$\eta = \frac{q}{j}$ **/ V**	**j / A m^{-1}**	Refs.	q, j_{used}
Entropic	PEMFC, anode	(0-0.72) · T/1000	(2-4)·10^4	(48, 49)	0.0002·T, 10^4
Entropic	PEMFC, cathode	(0.2-0.9)·T/1000	(2-4)·10^4	(48, 49)	0.0009·T, 10^4
Ohmic	PEMFC, membrane	(δ/2-δ/12)·j	(2-4)·10^4	(50, 53)	$\delta j^2/10$, 10^4
Tafel	PEMFC, cathode	0.4-0.55	(2-4)·10^4	(51)	0.5·j, 10^4
Entropic	LiB, anode	-2.4·T/1000	20-80	(52)	-0.0024·T, 60
Entropic	LiB, cathode	2.8·T/1000	20-80	(52)	0.0028·T, 60
Ohmic	LiB, separator	(1.5-2.5)·j/1000	20-80	(34)	$0.002 \cdot j^2$, 60
Tafel	LiB cathode	0.07-0.11	20-80	(34)	0.1, 60
Ohmic	SC, separator	(10^{-5}-10^{-4})·j	100-200	(47)	$10^{-5}j^2$, 200

*

discharging. The SC models consider continuous charging and discharging to balance another power electronic device (47). The range in resistance of an SC is attributed to what can be expected in an in-house device relative to a commercial one, and in the model we consider a value relevant for a commercial cell (10^{-4} S m^{-4}) (34).

Transport of heat leads to thermal gradients, both inside a cell and on the surface where a cooling fluid typically passes to adsorb the energy dissipated as heat. In this study, the primary consideration concerns the inside of the three technologies, but a comment to external gradients is also given, using flowing air or water as coolants. Natural thermal driven convection (*e.g.* rising air) has an effective heat transport coefficient of around 10 W K^{-1} m^{-2}, while forced air flow can have a heat transfer coefficient around 50 W K^{-1} m^{-2}. Flowing water on a flat surface, which is relevant as a lower value inside a PEMFC cooling channel, is 100 W K^{-1} m^{-2}.

Results and Discussion

There are several reasons for comparing the temperature gradients and thermal conductivity values of various storing technologies, as it is done here. In doing so, it is useful to first look at each technology individually and then thereafter do the complete comparison. This is as each technology is here presented by one example and each technology can in reality appear in a different shape, which affects heat management.

PEMFC Temperature Gradients

With reference to Fig. 1 and the two purple lines, we report the through-plane temperature profiles from under land (UL) or rib and under the gas channels (UC). The heat transfer in the gas channels are modelled based on a surface mass transfer coefficient and conduction in the bulk gas of the gas channel. This can be seen as an underestimation of cooling, as then most heat leaves via the in-plane direction of the GDL rather than via the gas channel. This is typical for a design where the PEMFC temperature control is based on cooling in the backing or polarisation plates rather than air cooling in the gas channels. In any of the two cases (backing plate inter cooling or gas channel cooling) the large in-plane thermal conductivity leads to relatively low temperature gradients (1-2 K per mm) in-plane in the membrane, CL and MPL. Moreover this in-plane temperature distribution is independent of whether the PEMFC components contain liquid water. The through plane temperature gradients under land (solid lines, U.L.) and the maximum temperature difference inside the PEMFC relies heavily on whether

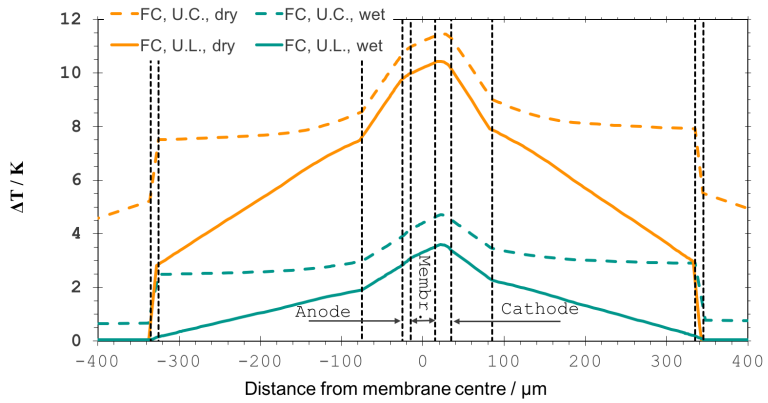

Figure 2. Temperature gradients (differences) inside a PEMFC, under land and under the gas channel, at 10 kA m^{-2} and 0.7 V.

liquid water is present (blue-green) or absent (red-orange). This is because of the enormous increase of thermal conductivity in the materials (a factor of 2-3) when water is present. As soon as water flows through a GDL or starts condensing near the under land region (as it is much colder there) the "wet" model considerations can be considered the most relevant. This effect persists during dry out, as tiny water droplets between fibres or fibre-backing continue to exist and create regions of high thermal conductivity for as long as there is some humidity in the PEMFC (25). In the light of this, the "wet" model is the most relevant for the PEMFC when considering thermal conductivity and temperature gradients.

Irrespective of water content, the heat flux transferred from the PEMFC to the cooling water channels is around 4300 W m^{-2} (half of $0.5 \cdot 10^4 + 0.0011 \cdot 300 \cdot 10^4 + 30 \cdot 10^{-6}/10 \cdot (10^4)^2$). With a backing inter-cooling plate where water streams through, so that each surface experiences this heat flux, the corresponding heat flux would be 43K ($4300[W/m^2]/100[W/m^2K]$). This points at, engineering cooling is as important inside the backing plate, if not more, as considering PEMFC internal temperature gradients. What is worth mentioning in this context, is that there is more room for engineering heat transfer in the backing cooling channels than what it is inside the PEMFC, and therefore PEMFC internal thermal models must be undertaken, even when the backing plate cooling is optimised.

LiB Temperature Gradients

A lithium ion battery (LiB) contains residual electrolyte, however, as the electrodes expand and contract during charging cycles, the level of residual electrolyte varies. Moreover, as LiB ages, the amount of residual electrolyte decreases. This means that the best case scenario for thermal gradients inside a LiB is the "wet" model, where the electrodes and separator swim in residual electrolyte. A worst case scenario is when the electrodes undergo a "dry out", either because the battery pack is vented or because the electrolyte is consumed by ageing. A representative situation for a LiB pouch can be that it is used in a up-right position so that the lower part is fully soaked in electrolyte (wet) and the upper part is partly dried out (something between "wet" and "dry"). Looking at Fig. 3, one can see that the modelled internal gradients inside a 24-cell (symmetry half is shown) pouch cell LiB does not give very large temperature gradients, with total temperature differences of less than 1 K (0.25 and 0.65K) over 3

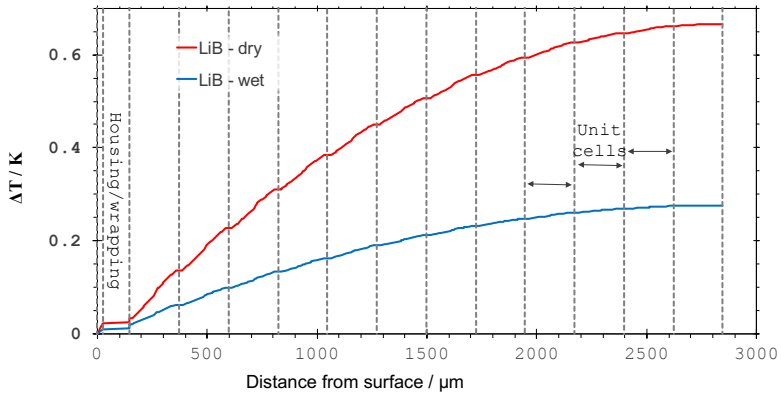

Figure 3. Temperature gradients (differences) inside a LiB given at 60 A m^{-2} (3c) continuous discharge.

mm.

LiB pouch cells, as modelled here, are often air cooled. Depending upon the flow regime of the air, the heat transfer coefficient is likely to vary between 10 and 50 W K^{-1} m^{-2}. Another strategy could be to immerse the entire stack in a non-conductive oil, like a power transformer, which would give a heat transfer coefficient of 100 W K^{-1} m^{-2}. An alternative to fluid cooling can be fins of aluminium with a compressible layer between the fin and the poach cell (as the battery expands and contracts during charging cycles). The compressible layer can be porous carbon, with likely thermal conductivity in the range of 0.1-0.5 W K^{-1} m^{-1}. Considering a thickness of 2-10 mm, the range of the heat transfer coefficient of such layer would be 10-250 W K^{-1} m^{-2}, which is quite similar to the range of fluid cooling. Considering the suggested heat source of a battery discharging at 3C (60 A m^{-2}) and that heat from 12 (of the 24 cells) pass through each of the two pouch surfaces, the surface heat flux becomes 245 W m^{-2} $(12 \cdot (0.0004 \cdot 300 \cdot 60 + 0.1 \cdot 60 + 0.002 \cdot 60^2))$. With a heat transfer coefficient range of 10-100 W K^{-1} m^{-2}, the external temperature drop of the battery becomes 2.5-25 K. Likewise with a PEMFC we see that the external temperature gradients are larger than the internal ones, and again that this is the part that can most easily be engineered to be smaller, while the internal gradients appear more as intrinsic properties of material and operation rate.

SC Temperature Gradients

A supercapacitor (SC) is similar to a LiB in that the dissipated energy from ohmic resistance is similar. The difference is that the current density is typically 3-5 times higher and that there is no dissipated energy from activation (Tafel or Butler-Volmer overpotential) as electrons are not exchanged between the electrode and reacting substances. In this example we have chosen an architecture for the SC that is the same as for the LiB, so that the comparison becomes easy. Looking at Fig. 4, we see that the internal temperature differences range from 0.05-0.25 for the electrode system soaked in electrolyte and the dry one, respectively. These are very small gradients and not really to be considered significant. From this point on, it is worth mentioning that most SC of large capacity are cylindrical and ten-fold in thickness compared to the present geometry. As reported earlier (45), temperature differences in a cylindrical design, using the same rate and irreversible losses as here, becomes more than ten times as much. This is

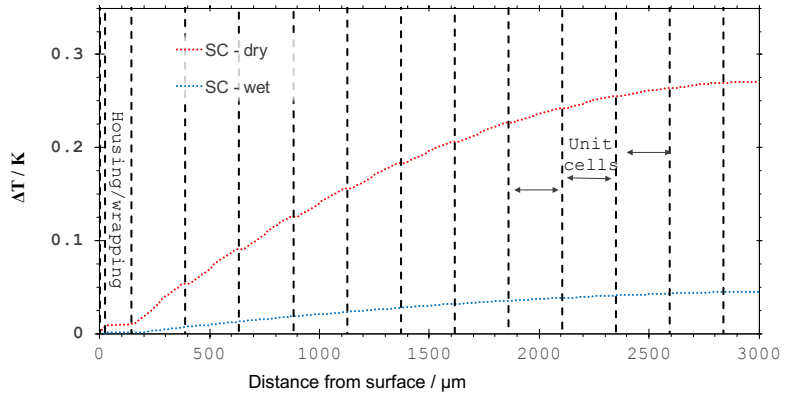

Figure 4. Temperature gradients (differences) inside an SC poach cell at 200 A m^{-2} and dynamic continous cycling.

not so surprising considering that the stack is ten times thicker. Of course, we see that the temperature difference increase over-linearly with thickness, but at the same time, a cylindrical design has an expanding area with radius, where the heat flux decreases with the radius. In this respect the second order polynomial temperature rise with thickness is weighed out by the logarithmic one of the cylindrical geometry, so that a linear dependency is fair as a first order of magnitude analysis between cylindrical thick SC with a prismatic thin SC. What does become a big difference is the heat flux at the surface of the two designs. If we consider a constraint where the total volume is kept constant in a pouch cell and a cylindrical design and that the height of the cylinder is equal to the width of the poach cell and a pouch cell of $0.15 \cdot 0.15 \cdot 0.007$ m3, the diameter would be 7.4 times the poach cell thickness and the surface area for cooling would be 2.6 times larger for the the poach cell. With a heat flux out of the SC poach cell of 48 W $m^{-2}(12 \cdot 10^{-5} \cdot 200^2)$ the equivalent would become around 125 W m^{-2}. Considering air flow or natural convection for the poach cell and the cylindrical cell, the external temperature drops would become 1-5 K and 3-13 K , respectively. Again, the lesson learnt is that external and "engineerable" cooling is the most important one, and it must be dealt with considering the internal temperature gradients on top of the external ones. Such geometric analysis is also valid for LiB, and explain partly why large cells have a poach design rather than a cylindrical one.

Comparing Temperature Gradients in Electrochemical Energy Storage Devices

Internal temperature differences in a PEMFC is one order of magnitude larger than those in LiB and SC. Considering that the thickness is a tenth and that the gradients are hundred times as large, this sounds reasonable. This is illustrated in Fig. 5, where the PEMFC under land (UL), LiB, and SC temperature gradients are shown for the dry case an d the wet case. The temperature gradients of the PEMFC are given by the right y-axis while the LiB and SC gradients are given belongs to the right y-axis, where the right axis have ten times as large values as the left axis. When considering wet systems (residual water or electrolytes), the PEMFC have ten-fold temperature differences of LiB and SC. This can be understood from the fact that the PEMFC has hundred times higher rates than the other technologies, a tenth in number of active stacked active cells, and with very similar thermal conductivities.

When revising the external temperature gradients it is clear that large temperature

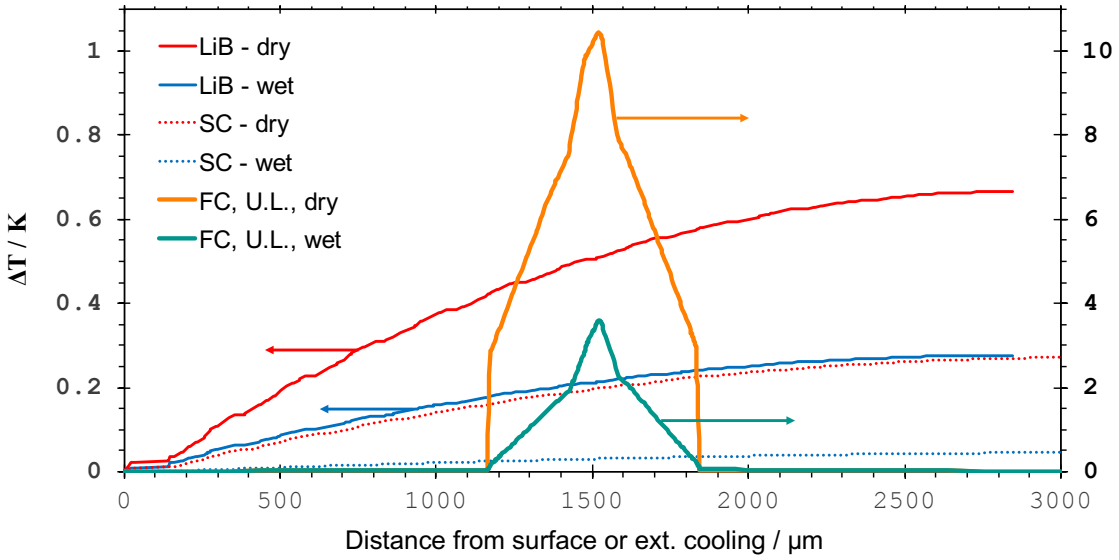

Figure 5. Temperature gradients (differences) inside a dry and wet PEMFC (under land), LiB, and SC, as otherwise presented in Figs. 2-4. The PEMFC temperatures are given by the right y-axis and the LiB and SC temperatures by the left y-axis.

gradients emerge in cooling air or cooling water. This is however something that can be engineered by different means, like surface modifications. In doing so, this study shows that internal temperature gradients must also be accounted for in a PEMFC, a LiB, and an SC, although it is of less importance for SC flat poach cells.

Conclusions

In terms of thermal conductivity, the materials of PEMFC, LiB, and SC have a lot in common. They are porous and fully or partly soaked with a liquid, which defines the thermal conductivity of the electrodes materials in the range of 0.4-1.5 W K^{-1} m-1 and the electrolyte or separator in the range of 0.2-0.5 W K^{-1} m-1.

In terms of conversion rate or current density the three differ significantly, which is the main reason why the PEMFC experiences ten times as high internal temperature variations as the LiB and the SC.

The PEMFC also experiences much higher irreversible energy losses than the other technologies, but this is compensated by having cooling in between every cell in a PEMFC, whereas LiB and SC typically are stacked or rolled in ten-folds of layers.

Air and water cooling appear to be the most important factor for controlling the temperature differences in all the systems, as long as a flat surface laminar flow is considered.

Acknowledgement

Financial support from ENERSENSE (Energy and Sensor Systems) group at the Norwegian University of Science and Technology (NTNU) is greatly acknowledged.

References

1. Odne S. Burheim. *Engineering Energy Storage*. Academic Press, Elsevier, 1st edition, 2017. ISBN 9780128141007.
2. N. Zamel and Xiangou Li. *Progress in Energy and Combustion Sci.*, **39**:111–146, (2013).
3. O. S. Burheim and J. G. Pharoah. *Current Opinions in Electrochem.*, **5**:36–42, (2017).
4. F. Nandjou, J.-P. Poirot-Crouvezier, M. Chandesris, J.-F. Blachot, C. Bonnaud, and Y. Bultel. *ECS Trans.*, **66**:1–12, (2015).
5. A.A. Kulikovsky. *J. Electroan. Chem.*, **652**:66–70, (2011).
6. T. Waldmann, M. Wilka, M. Kasper, M. Fleischhammer, and M. Wohlfahrt-Mehrens. *J. Power Sources*, **262**:129–135, (2014).
7. F. Richter, S. Kjelstrup, P.J.S. Vie, and O.S Burheim. *J. Power Sources*, **359**:592–600, (2017).
8. S. Porada, R. Zhao, A. van der Wal, V. Presser, and P.M. Biesheuvel. *Progress in Mat. Sci.*, **58**:1388–1442, (2013).
9. P.J.S. Vie and S. Kjelstrup. *Electrochim. Acta*, **49**:1069–1077, (2004).
10. M. Khandelwal and M. M. Mench. *J. Power Sources*, **161**:1106–1115, (2006).
11. J. Ramousse, O. Lottin, S. Didierjean, and D. Maillet. *Int. J. Thermal Sci.*, **47**:1–6, (2008).
12. O. Burheim, H. Lampert, J.G. Pharoah, P.J.S. Vie, and S. Kjelstrup. *J. Fuel Cell Sci. and Technol.*, **8**:021013–1–11, (2011).
13. O. Burheim, P.J.S. Vie, J.G. Pharoah, and S. Kjelstrup. *J. Power Sources*, **195**: 249–256, (2010).
14. E. Sadeghi, N. Djilali, and M. Bahrami. *J. Power Sources*, **196**:3565–3571, (2011).
15. P. Teertstra, G. Karimi, and X. Li. *Electrochim. Acta*, **56**:1670–1675, (2011).
16. N. Zamel, E. Litovsky, S. Shakhshir, X. Li, and J. Kleiman. *Appl. Energy*, **88**: 3042–3050, (2011).
17. N. Alhazmi, M.S. Ismail, D.B. Ingham, K.J. Hughes, L. Ma, and M. Pourkashanian. *J. Power Sources*, **241**:136–145, (2013).
18. O. S. Burheim, G. Ellila, J. D. Fairweather, A. Labouriau, S. Kjelstrup, and J. G. Pharoah. *J. Power Sources*, **221**:356–365, (2013).
19. A. Thomas, G. Maranzana, S. Didierjean, J. Dillet, and O. Lottin. *Int. J. of Hydrogen Energy*, **39**:2649–2658, (2014).
20. M. Andisheh-Tadbir, E. Kjeang, and M. Bahrami. *J. Power Sources*, **296**:344–351, (2015).
21. O.S. Burheim, H.Su, S.Pasupathi, J.G. Pharoah, and B.G. Pollet. *Int. J. Hydrogen Energy*, **38**:8437 – 8447, (2013).
22. O.S. Burheim, G.A. Crymble, R. Bock, N. Hussain, S. Pasupathi, A. Plessis, S. le Roux, F. Seland, H. Su, and B.G. Pollet. *Int. J. Hydrogen Energy*, **40**, (2015).
23. O.S. Burheim, H. Su, H.H. Hauge, S. Pasupathi, and B.G. Pollet. *Int. J. Hydrogen Energy*, **39**:9397–9408, (2014).
24. G. Xu, J. M. LaManna, and M. M. Mench. *J. Power Sources*, **256**:212–219, (2014).
25. Andrew D. Shum, Dilworth Y. Parkinson, Xianghui Xiao, Adam Z. Weber, Odne S. Burheim, and Iryna V. Zenyuk. *Electrochim. Acta*, **256**:279–290, (2017).
26. N. Zamel, E. Litovsky, S. Shakhshir, X. Li, and J. Kleiman. *Int. J. Hydrogen Energy*, **36**:12618–12625, (2011).
27. M. Ahadi, M. Tam, M.S. Saha, J. Stumper, and M. Bahrami. *J. Power Sources*, **354**:207–214, (2017).

28. R. Bock, A.D. Shum, X. Xiao, H. Karoliussen, F. Seland, I.V. Zenyuk, and O.S. Burheim. *J. The Electrochem. Soc.*, **165**:F514–F525, (2018).
29. O. S. Burheim. *ECS Trans.s*, **80**:509–525, 2017.
30. S.G. Kandikar and Z. Lu. *J. Fuel Cell Sci. and Technol.*, **6**:04401–1–13, (2009).
31. C.J. Bapat and S.T. Thynell. *ASME, J. Heat Transfer*, **129**:1109–1118, (2007).
32. G. Aylward and T. Findlay. *SI Chemical Data*. Wiley, New York-, 5th edition, 2002.
33. T.M. Bandhauer, S. Garimella, and T.F. Fuller. *J. the Electrochem. Soc.*, **158**:R1–R25, (2011).
34. O.S. Burheim, M.A. Onsrud, J.G. Pharoah, F. Vullum-Bruer, and P.J.S. Vie. *ECS Trans.*, **58**:145–171, (2014).
35. F. Richter, S. Kjelstrup, P.J.S. Vie, and O.S. Burheim. *Electrochim. Acta*, **250** : 228–237, (2017).
36. A. Loges, S. Herberger, D. Werner, and T. Wetzel. *J. Power Sources*, **325**:104–115, (2016).
37. S.J. Bazinski, X. Wang, B.P. Sangeorzan, and L. Guessous. *Energy*, **114**:1085–1092, (2016).
38. H. Maleki, S. Al Hallaj, J.R. Selman, R.B. Dinwiddie, and H. Wang. *J. the Electrochem. Soc.*, **146**:947–954, (1999).
39. D. Werner, A. Loges, D.J. Becker, and T. Wetzel. *J. Power Sources*, **364**:72–83, (2017).
40. E. Barsoukov, J.H. Jang, and H. Lee. *J. Power Sources*, **109**:313–320, (2002).
41. K.A. Murashko, A.V. Mityakov, J. Pyrhönen, V.Y. Mityakov, and S.S. Sapozhnikov. *J. Power Sources*, **271**:48–54, (2014).
42. K.A. Murashko, A.V. Mityakov, V.Y. Mityakov, S.Z. Sapozhnikov, and J. Pyrhönen. In *Power Electronics and Applications (EPE'17 ECCE Europe), 2017 19th European Conference on*, pages P–1. IEEE, (2017).
43. S. He, B.T. Habte, and F. Jiang. *Int. Comm. Heat and Mass Transf.*, **82**:1–8, (2017).
44. H.H. Hauge, V. Presser, and O. Burheim. In-situ and ex-situ measurements of thermal conductivity of supercapacitors. *Energy*, 78:373–383, 2014.
45. O.S. Burheim, M. Aslan, J.S. Atchison, and V. Presser. *J. Power Sources*, **246**:160 – 166, 2014.
46. A. Xiong, G.and Kundu and T.S. Fisher. In *Thermal Effects in Supercapacitors*, pages 115–141. Springer, (2015).
47. A. d'Entremont and L. Pilon. *J. Power Sources*, **246**:887–898, (2014).
48. O. Burheim, S. Kjelstrup, J.G. Pharoah, P.J.S. Vie, and S. Møller-Holst. *Electrochim. Acta*, **5**:935–942, (2011).
49. S. Kjelstrup, P. J. S. Vie, L. Akyalcin, P. Zefaniya, J.G. Pharoah, and O. S. Burheim. *Electrochim. Acta*, **99**:166–175, (2013).
50. T. E. Springer, T. A. Zawodzinski, and S. S. Gottesfeld. *J. Electrochem. Soc.*, **138**: 2334–2343, (1991).
51. O. Burheim, P.J.S. Vie, S. Møller-Holst, J.G. Pharoah, and S. Kjelstrup. *Electrochim. Acta*, **5**:935–942, (2010).
52. F. Richter, A. Gunnarshaug, O.S. Burheim, P.J.S. Vie, and S. and Kjelstrup. *ECS Trans.*, **80**:219–238, (2017).
53. J.G. Pharoah and O.S. Burheim. *J. Power Sources*, **195**:5235–5245, (2010).